Crystal Structure-Mechanical Property Relationship in Succinic acid and L- alanine Probed by Nanoindentation

Sushmita Majumder, ¹ Tianyi Xiang, ² Changquan Calvin Sun, ^{2,*} Nathan A. Mara ^{1,*}

¹Department of Chemical Engineering and Materials Science, University of Minnesota, Minneapolis, MN 55455

Emails: sunx0053@umn.edu, mara@umn.edu

² Pharmaceutical Materials Science and Engineering Laboratory, Department of Pharmaceutics, University of Minnesota, Minneapolis, MN 55455

Abstract:

1

2

3

4

5

6

7

8

9

10

11

12

13

14

15

16

17

Establishing structure-mechanical property relationships is crucial for understanding and engineering the performance of pharmaceutical molecular crystals. In this study, we employed nanoindentation, a powerful technique that can probe mechanical properties at the nanoscale, to investigate the hardness and elastic modulus of single crystals of succinic acid and L-alanine. Nanoindentation results reveal distinct mechanical behaviors between the two compounds, with L-alanine exhibiting significantly higher hardness and elastic modulus compared to succinic acid. These differences are attributed to the underlying variations in molecular crystal structures - the three-dimensional bonding network and high intermolecular interaction energies of L-alanine molecules leads to its stiffness compared to the layered and weakly bonded crystal structure of succinic acid. Furthermore, the anisotropic nature of succinic acid is reflected in the directional dependence of the mechanical responses where it has been found that the (111) plane is more resistant to indentation than (100). By directly correlating the nanomechanical properties obtained from nanoindentation with the detailed crystal structures, this study provides important insights into how differences in molecular arrangements can translate into different macroscopic mechanical performance. These findings have implications on the selection of molecular crystals for optimized drug manufacturability.

18

19 20

21

22

24

Keywords: molecular crystal, anisotropy, nanoindentation, structure-property correlation,

23 intermolecular interaction energy

1. Introduction

Molecular crystals are ubiquitously used in the pharmaceutical industry as active pharmaceutical ingredients (APIs) in manufacturing solid dosage forms of drugs (Kumar Bandaru et al., 2021). The structural packing features of these crystals along with the strength of different types of intermolecular interactions determine their mechanical properties, which in turn influence pharmaceutical operations, such as milling (wet and dry) and tableting (Reddy et al., 2010, Datta et al., 2004). For instance, compaction of APIs into tablets will greatly depend on the material's ability to deform plastically (Egart et al., 2014). The requirement for relatively large quantities of APIs limits industrial-scale experimental trials, which cost substantial processing time and resources. Thus, there is a pressing need to reliably predict the bulk powder processability for improved drug manufacturing based on an established crystal structure-mechanical property correlation through systematic investigation of the mechanical properties of these APIs at the single-crystal level.

Collecting meaningful mechanical property datasets for molecular crystals requires special consideration and effort compared to engineering materials. Crystals are generally grown at small length scales (sub-mm sizes). Hence, shaping/machining the crystals to a specific geometry required for conventional mechanical test methods is difficult, if not impossible (Maughan et al., 2015). Nanoindentation has emerged as a powerful characterization tool for measuring a wide variety of mechanical properties, including but not limited to elastic modulus (*E*) and hardness (*H*), based on Hertz contact theory (Johnson et al., 1982) and the Oliver-Pharr analysis method (Oliver and Pharr, 1992). This method can measure load and displacement with resolutions of 1 nN and 0.2 nm, respectively, over deformed volumes as small as 1 µm³. As such, it is aptly suited for small, flat samples of different sizes and shapes (Schuh, 2006, Varughese et al., 2013). Comprehensive reviews of the nanoindentation working principle, its major developments in testing protocols, and challenging factors are available in the literature (Fischer-Cripps, 2011, Gouldstone et al., 2007, Majumder et al., 2022).

Several examples established nanoindentation as a reliable method for studying the elastic and plastic properties of molecular crystals, such as sucrose (Ramos and Bahr, 2005), acetaminophen

(Liao and Wiedmann, 2005), ascorbic acid, tartaric acid, glycine, acetylsalicylic acid (Meier et al., 2009), explosive molecular crystals (Bahr et al., 2009, Bahr et al., 2017, Bahr et al., 2020) and various co-crystals (Bhukkal et al., 2018, Mondal et al., 2020). Maughan and his group (Maughan et al., 2015) showed that elastic-plastic indentation with a 3-sided pyramidal Berkovich probe is the most appropriate approach to quantify modulus (E) and hardness (H) due to the minimum effect of surface angle and roughness. In a recent study, Bahr showed how nanoindentation reveals the mechanical footprint of azodiaminoazoxyfurazan (ADAAF), and 1,3,5-triamino-2,4,6trinitrobenzene (TATB) which are molecular crystals of explosive nature (Bahr et al., 2023). Effect of water on the mechanical properties were investigated with anhydrous and hydrated uric acid to understand how kidney stones might deform (Swift et al., 2018). Furthermore, hydration effect on the mechanical properties were explored by several other researchers to understand their impact on tabletability (Sun and Grant, 2004, Malaj et al., 2010,). Crystal anisotropy was demonstrated by determining E and H in different crystal faces using nanoindentation (Varughese et al., 2013). Anisotropy in plastic deformation and fracture behavior was also explored (Kiran et al., 2010), where the observed mechanical response to crystal structure in terms of slip systems and interaction strengths were correlated. It was also shown that the onset of plasticity or yielding occurs at stresses within approximately 1-5% of the reduced modulus value for a wide range of organic crystals (Taw et al., 2017). Indentation-based mechanical properties were correlated with underlying packing arrangement in molecular crystals and this correlation then may be used to predict tableting (Chattoraj et al., 2010) and milling behavior (Meier et al., 2009, Taylor et al., 2004). Even though the number of published works on structure-property correlation is rising, this field is not yet fully explored. Consequently, a clear understanding of the crystal structure mechanical property - performance relationship is required to inform reliable milling and tableting process models.

80

81

82

83

84

85

86

56

57

58

59

60

61

62

63

64

65

66

67

68

69

70

71

72

73

74

75

76

77

78

79

In this work, we aim to expand the knowledge base for establishing such structure – property – processing – performance relationships by investigating the mechanical properties of two molecular crystals, i.e., succinic acid (SA) and L-alanine (LA), employing the high-throughput nanoindentation technique at ambient condition. The softer SA and harder LA were chosen as model materials for their contrasting mechanical characteristics. Given the importance of anisotropy of molecular crystals in interpreting their complex deformation behaviors, we also

performed indentation on different crystal planes of SA and LA to understand how the indentation direction affect mechanical responses. Finally, we analyzed the work-hardening propensity in these crystals due to prior surface deformation to gain a deeper insight into work hardening behavior, which becomes important for materials undergoing deformation to large strains as in tableting, and/or multiple loading events as for milling.

2. Materials and methods

2.1 Synthesis of molecular crystals

Single crystals of succinic acid (C₄H₆O₄) and L-alanine (C₃H₇NO₂) were prepared by the cooling crystallization method. 0.8 grams commercial powder of succinic acid (99% purity, Thermo Scientific Chemicals, Waltham, MA, USA) was introduced into 10 mL water to form a suspension at room temperature. After heating up until all the dispersed particles dissolved and cooling back to room temperature, an aqueous solution with 115% supersaturation degree was produced, and one single seed crystal of succinic acid was introduced into the solution initiate crystal growth. A similar procedure was done to L-alanine (99% purity, Sigma-Aldrich, St. Louis, MO, USA) with 1.8 grams starting powder and 10 mL water, to form 108% supersaturated solution at room temperature. Seeds were also applied for initiating single crystal growth of L-alanine. After growing for about 2 weeks, the crystals were isolated from the solution and air-dried at room temperature after wiping the excess liquid on the surfaces. The crystal sizes and shapes were uniform with succinic acid being hexagonal and L-alanine forming trapezoidal crystals. Images of these crystals were taken with an optical microscope (Nikon Eclipse E200). The crystals were affixed on the metal disc using the small crystal method (Maughan et al., 2015) to ensure a flat surface perpendicular to the indenter axis.

Crystallographic files were downloaded from the Cambridge Structural Database (Groom et al., 2016). Succinic acid (refcode: SUCACB08 (Gopalan et al., 2000)) grows into a monoclinic (β form) space group of $P2_1/a$ with unit cell lengths of a=5.477 Å, b=8.790 Å, c=5.027 Å, and a cell angle of $\beta=92.91^{\circ}$. L-alanine crystal (refcode: LALNIN22 (Wilson et al., 2005)) is in an orthorhombic space group of $P2_12_12_1$ with cell parameters of a=6.036 Å, b=12.342 Å, c=5.788 Å.

2.2 Crystal face indexing

Crystal faces for indentation were indexed with a Bruker D8 Discover X-ray Diffractometer using monochromatic Co-K α (1.79 Å) radiation at 40 kV voltage and 35 mA current. Samples were mounted on a metal disc using epoxy and positioned on the XYZ stage of the diffractometer. The sample remained stationary while the source and detector moved independently. The effect of surface curvature was minimized by using a small beam size of 0.3 mm. Scans were collected with the omega scan mode at room temperature over a 20 range of 5-40° and peaks were analyzed using the JADE software.

2.3 Powder X-ray diffractometry (PXRD)

- 128 Bulk powder phase purity was evaluated using a powder X-ray diffractometer (X'Pert PRO,
- 129 PANalytical Inc., West Borough, MA) with a Cu- Kα (1.5406 Å) radiation at 45 kV and 40 mA
- over a 2θ ranging from 5° to 35° and a 0.017° step size. PXRD patterns were also calculated from
- 131 crystal structures using Mercury (V. 2023.2.0, CCDC, Cambridge, UK).

2.4 Nanoindentation

Nanoindentation data were collected using a nanoindenter (TI 980, Hysitron, Eden Prairie, MN) at ambient conditions and analyzed using the Oliver-Pharr method (Oliver and Pharr, 1992). A diamond Berkovich probe was used to measure E and H of the crystals. Indentations were conducted in load-controlled mode with a partial load-unload function having 1 s load, 5 s hold, and 0.5 s unload segments with a peak load of $1000 \, \mu N$. To alleviate possible creep effects on the unloading stiffness that are often seen during indentation of molecular crystals, we ensured that the unloading rate was at least 20x the creep rate. To evaluate the effect of pre-deformation on mechanical behavior, a quasi-static load with displacement-controlled mode was employed with a cylindrical probe of $20 \, \mu m$ diameter and then Berkovich indentation was performed on the pre-deformed zone. Samples were not aligned to any particular orientation during indentation. Prior to indentation, the cross-sectional tip-area function was calibrated using fused quartz with known elastic modulus and hardness to ensure valid measurements and reliable data collection. Indents were made on suitable surface locations with a root mean square (RMS) surface roughness less than 3 nm over an area of $20 \times 20 \, \mu m$ and a tilt not greater than 3° . A minimum of 15 indentations were carried out on each of the crystals. Values for hardness and modulus were calculated from

averages of several indents over a depth range free from indentation size or surface roughnesseffects.

151

152

2.5 Surface topography analysis

- 153 Crystal surfaces were scanned using an *in-situ* scanning probe microscope (SPM) equipped with 154 the Hysitron TI 980 before indentation to ensure a flat, smooth surface conducive to the
- experiment. A scan rate of 0.5 Hz was used to minimize surface abrasion. Post-SPM scans were
- analyzed using an open-source software Gwyddion 2.65 (Nečas and Klapetek, 2012).

157

158

2.6 Structure visualization and surface rugosity calculation

- Molecular packing features were analyzed using VESTA 3.5.7 (Momma and Izumi, 2011).
- Visualization of crystallographic planes and directions parallel to the indentation axis aided in
- 161 correlating structural features with mechanical properties. Surface rugosities of crystal planes are
- quantified using the CSD Python API software in Mercury (Macrae et al., 2008).

163

164

2.7 Calculation of BFDH morphology and attachment energies

- 165 The Bravais-Friedel-Donnay-Harker (BFDH) morphologies were calculated with the software
- 166 BIOVIA Materials Studio 2022 (Accelrys, San Diego, CA) (Dassault 2022), using the crystal
- structures. Attachment energies were obtained with the Forcite module, Dreiding forcefield, and
- 168 charges Q_{eq} at ultrafine quality. The "Ewald" electrostatic summation method and "atom based"
- 169 van der Waals summation were chosen for this work.

170171

2.8 Calculation of energy framework

- 172 The intermolecular interaction energies in SA and LA were calculated using CrystalExplorer 21.3
- 173 (Spackman et al., 2021) with the B3LYP-D2/6-31G(d,p) molecular wavefunction. The total
- 174 intermolecular interaction energy is the sum of electrostatic, polarization, dispersion, and
- exchange-repulsion components with scaling factors of 1.057, 0.740, 0.871, and 0.618,
- 176 respectively. The cylinder thickness that is proportional to the interaction energies was set to 50
- and no cut-off energy was specified.

178

179

3. Results and discussion

3.1 Crystal morphology and face indexing

Crystal habit strongly influences downstream pharmaceutical processes, such as comminution, compaction, and dissolution rate of drugs (Storey, 2011, Sun and Grant, 2001, Modi et al., 2014). As represented in **Fig. 1a**, the BFDH model predicts a hexagonal morphology of SA with (011) and (100) being the dominant faces. The (011) face has the slowest growing rate and the largest total habit facet area (40.13%), making it morphologically most dominant. The (100) face possesses the second-largest facet area (24.20%). The experimentally grown SA crystal, in **Fig 1b**, has a hexagonal shape with (100) being the face having the largest surface area and, thus, the most accessible crystal face to indent.

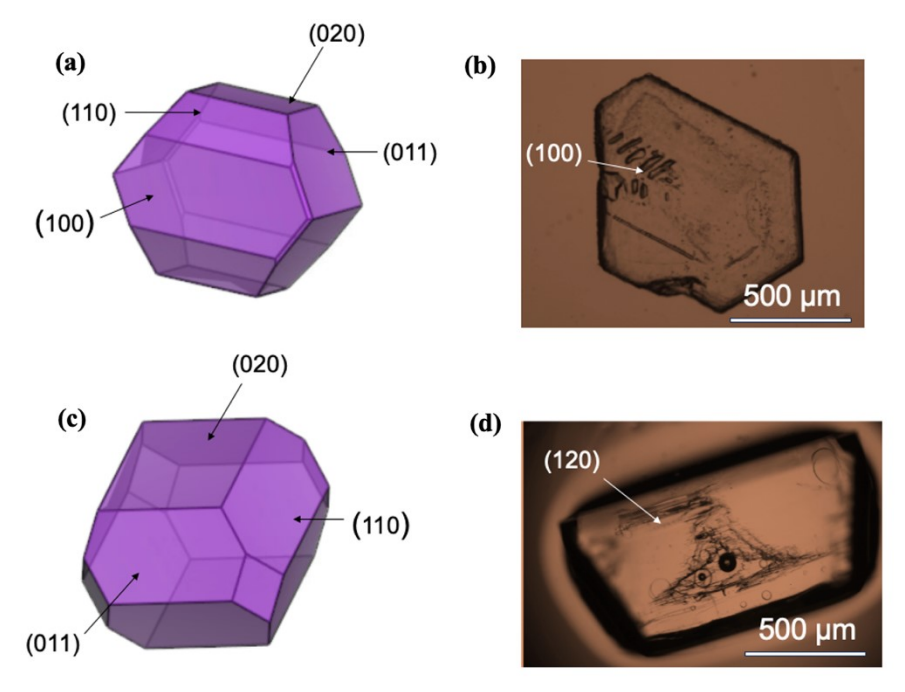


Fig. 1. a) Predicted morphology of SA, b) Experimentally grown single crystal of SA showing major habit plane (100), c) Predicted morphology of LA, d) Experimentally grown single crystal of LA showing major habit plane (120).

The predicted (**Fig. 1c**) and the experimental (**Fig. 1d**) morphology of LA show some differences. The BFDH facet surface area of the two dominant faces was 36.85% for (011) and 34.68% for (110). The grown LA crystal possesses a trapezoidal morphology and the largest crystal face was (120). The crystals of SA and LA were cleaved with a sharp razor to access other faces for indent. Other minor faces were not conducive for indentation as the surfaces were not sufficiently flat and smooth.

The experimental PXRD patterns of SA and LA powders were compared with the simulated PXRD patterns confirming that these were phase pure (Fig. S1). The crystal faces on which indentation were performed, i.e., the most prominent growth face (100) and the cleaved face (111) of SA were confirmed from their 2θ angles (Fig. 2). Similarly, LA has as the growth face (120) and the cleaved face (111), respectively.

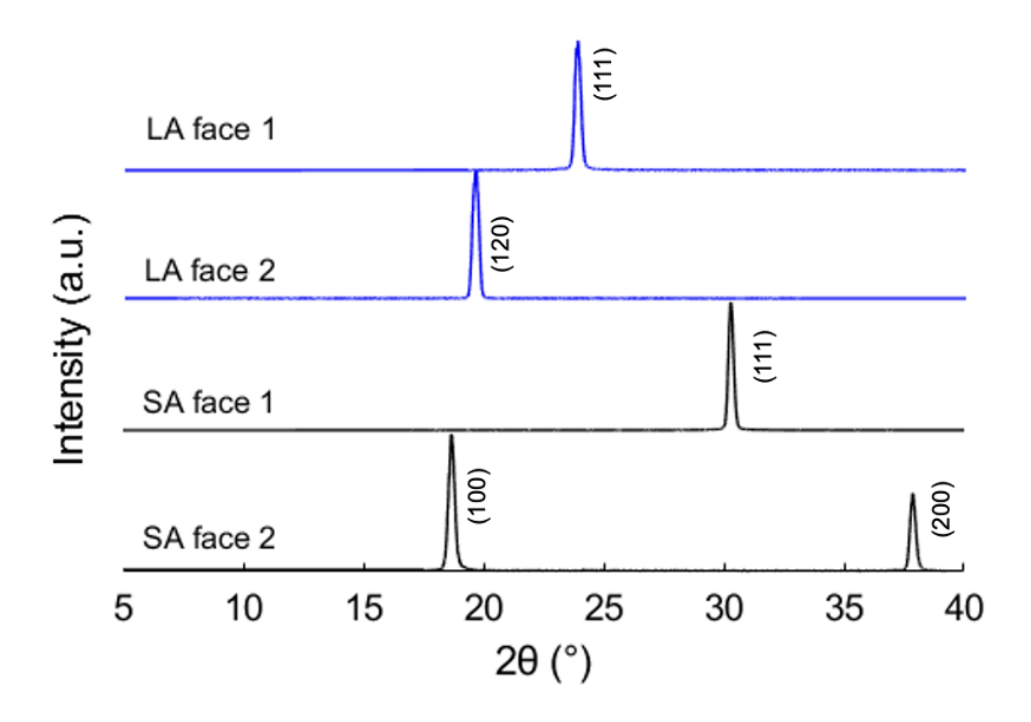
205 206

201

202

203

204



207 208

Fig. 2. Single crystal X-ray diffraction patterns of succinic acid (SA) and L-alanine (LA) identifying the faces for nanoindentation.

209 210

211

212

3.2 Mechanical property analysis by nanoindentation

213 214

215 216

217 218

219 220

Representative load-displacement (P-h) plots for the two faces of SA and LA are shown in Fig. 3. Significant plastic deformation took place in all the crystals as given by the large residual depths upon unloading. (100) in SA has higher penetration depth than (111) at the same peak load, which indicates a softer nature of (100) than (111). Both the curves of LA attain more similar maximum depth showing similar deformation pattern. There are several displacement bursts or 'pop-ins' observed along the loading segments of the P-h curves, which are commonly observed in molecular crystals lacking sufficient slip systems and undergoing heterogeneous plastic deformation (Xia et al., 2016, Lorenz et al., 2003).

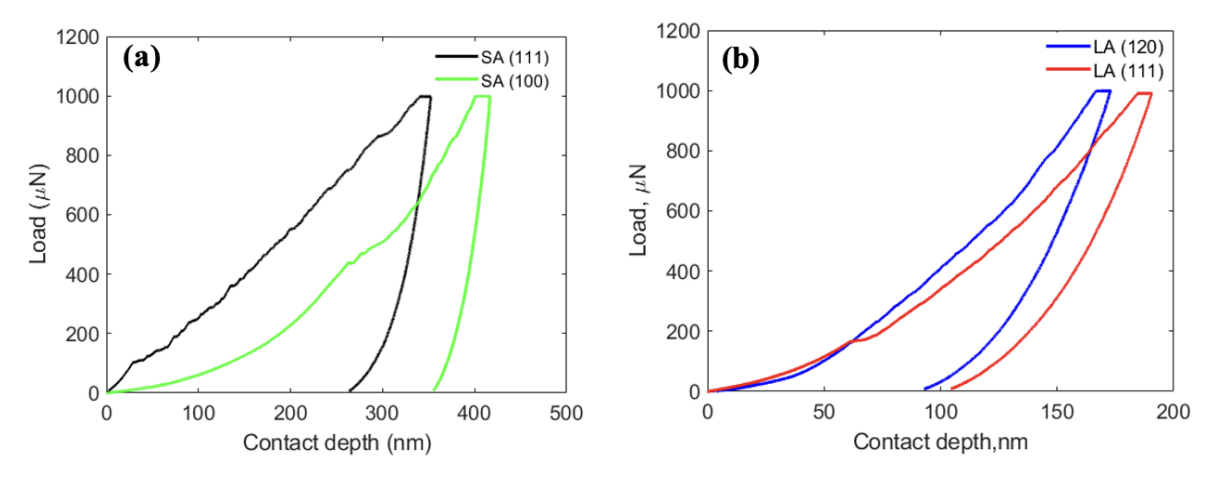


Fig. 3. Representative *P-h* plots of (a) SA and (b) LA for different faces obtained from nanoindentation.

When measuring the modulus and hardness, a partial load-unload function was used to measure depth-dependent properties. The E and H values at shallow contact depth generally have disparity due to the effect of surface roughness and indentation size effects (**Fig. S2**). As indentation progresses deeper into the material, the E and H values become independent of the displacement and attains a plateau. Thus, the property values were averaged in this plateau region for each test and the truncated data has been shown in (**Fig. 4**).

Table 1 Summary of E, H and H/E for succinic acid (SA) and L-alanine (LA), (n = 15).

Crystals	Indented	E (GPa)	E (GPa)	H (GPa)	H (GPa)	H/E
	face		(deformed		(deformed	
			surface)		surface)	
SA	(100)	11.10 ± 0.69	19.76 ± 2.11	0.40 ± 0.01	0.50 ± 0.09	0.036
	(111)	15.58 ± 0.19		0.48 ± 0.02		0.031
LA	(120)	25.50 ± 0.86	23.2 ± 1.73	1.65 ± 0.02	1.22 ± 0.2	0.065
	(111)	19.74 ± 0.43		1.09 ± 0.02		0.055

It is important to note that the reported error bars of the hardness and modulus data are standard deviations in the values, which are higher than that associated with instrumentation noise. Hence, they are associated with variability in the measured behavior or property, as opposed to instrument

error. Given the roughness of our crystal surfaces, and the tendency of the data to reach a similar asymptotic value at greater depths, we attribute this variability to differences in contact conditions at different test locations.

Different E values for indentation on different crystal planes in SA and LA suggest interaction anisotropy (**Table 1**). Both E and H of (100) plane in SA is lower than that of (111). Similarly, in LA, (120) has higher E and H than (111), apparently suggesting anisotropy in both properties. E and E values measured in this study are comparable to previously reported values of LA, i.e., E (25.1 \pm 0.28 GPa for (001) face and 19.2 \pm 0.54 GPa for (101) face, ranging from \sim 19-25 GPa) and E (1.1 \pm 4.8 GPa for (001) face and 0.9 \pm 3.1 GPa for (101) face, ranging from \sim 1-2 GPa, (Mohamed et al., 2015). Therefore, LA has a relatively isotropic nature. E ratios are also calculated to as an estimate of relative brittleness. As expected, LA has a significantly higher E ratio than SA.

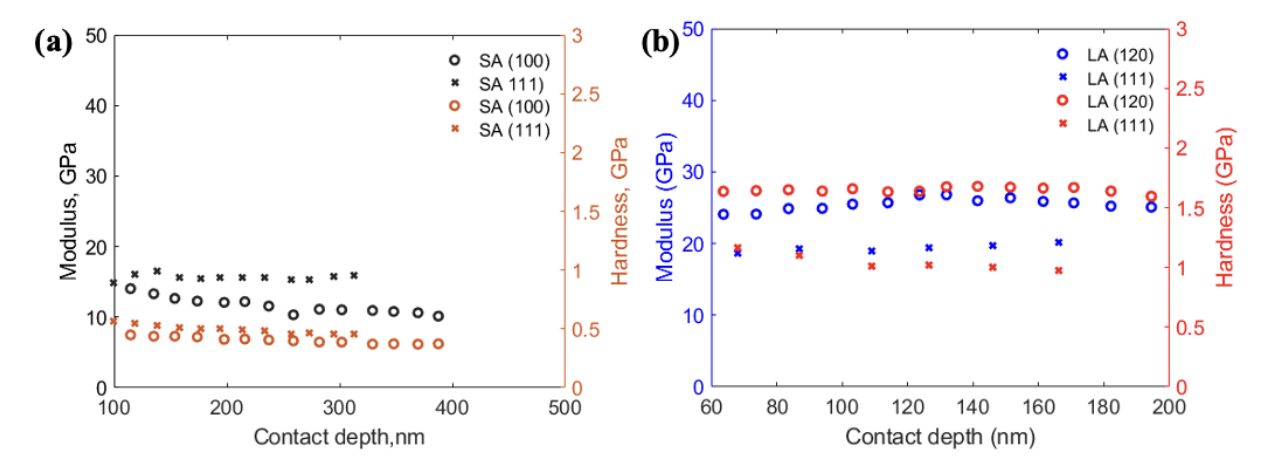


Fig. 4. Modulus and hardness plots for the crystal faces (a) (100) and (111) in SA (b) (120) and (111) in LA. A single representative data for each of the faces is shown here over a range of depth where E and H are constant.

L-alanine is both significantly harder (based on H) and stiffer (based on E) than succinic acid. This is also evident by the deeper indenter displacement in succinic acid (>300 nm) than that in L-alanine (<200 nm) for the same peak load of 1000 μ N (**Fig. 3**). Thus, L-alanine is more resistant to plastic deformation. A low H/E value was thought to favor a better compaction behavior (Duncan-Hewitt and Weatherly, 1989, Sanphui et al., 2015). Based on this, SA is expected to

exhibit better compaction properties than L-alanine. On the other hand, a crystal with a very low *H* is more difficult to undergo size reduction by milling (Mishra et al., 2016). Therefore, a judicious selection of mechanical properties is required to simultaneously maintain adequate millability and tabletability.

Pile-up (material rising above the surface) and sink-in (material sinking into the surface) are two phenomena that can be encountered during nanoindentation. As a result of change in contact depth and area, H can get overestimated due to pile-up or underestimated due to sink-in. SPM images of the impressions post-indent were obtained to evaluate potential impact by these phenomena (**Fig. 5**). SA shows no pile-up of material (**Fig. 5a**), but L-alanine shows some degree of pile-up around the indent edges (**Fig. 5b**). In assessing the possibility of overestimating H of LA due to pile-up, we calculated h_f/h_{max} of LA, where h_f is the final displacement attained after complete unloading, and h_{max} is the maximum depth of penetration. The h_f/h_{max} calculation rules out any appreciable impact of pile-up on the H value as it is less than 0.7 (Bolshakov and Pharr, 1998, Gale and Achuthan, 2014).

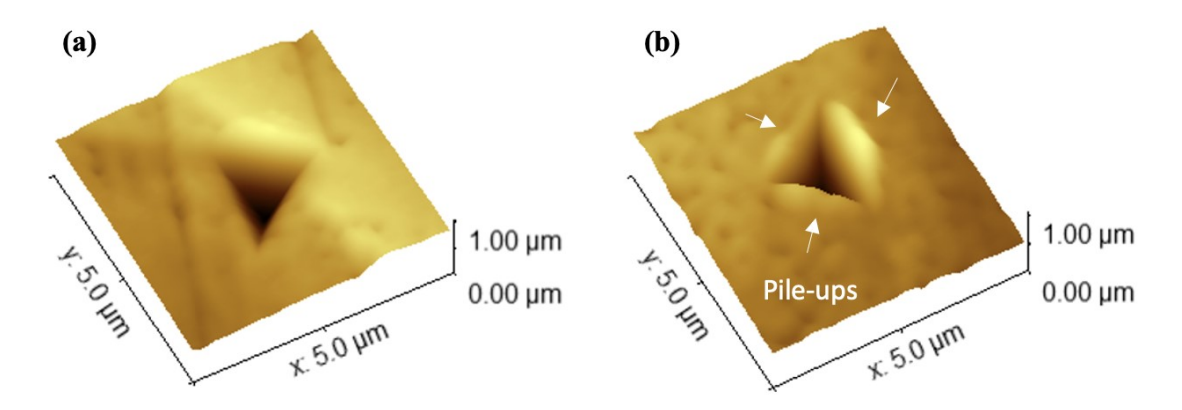


Fig. 5. Topographical SPM images of (a) SA and (b) LA. LA shows pile up around the indent edges. Here, lighter colors correspond to higher topography.

3.3 Work hardening propensity

During tablet manufacturing, API crystals are subjected to two key mechanical stresses, the first is during size reduction and the second is during compaction (Rajkumar et al., 2019). When the applied stress exceeds a certain value, crystals deform plastically. However, if a material requires

an increased stress for continued deformation it is said to have been work hardened (Clarebrough and Hargreaves, 1959). Work hardening of materials during milling may lead to a loss in compactibility (Rajkumar et al., 2019, Sun and Kleinebudde, 2016). Thus, it is useful to analyze the work hardening propensity of these crystals to understand their performance during the entire tablet manufacturing process. While several experimental and computational analyses of work hardening are available for high symmetry crystals (Nabarro, 1989, Mitchell et al., 1963, Zepeda-Ruiz et al., 2021) and a few theoretical studies for energetic molecular crystal (Khan and Picu, 2021), there is no published experimentally work on the work hardening phenomenon in molecular crystals.

We investigated work hardening propensity of SA and LA using the versatility of nanoindentation. The (100) face of SA and (111) face of LA were first deformed to a depth of 1500 nm (displacement-controlled) using a flat punch/cylindrical probe of 20 µm diameter and then indented with a Berkovich tip afterward (**Fig. 6**). Compared to the *E* and *H* values of the pristine crystal faces, pre-deformed SA showed a moderate increase in *E* and *H* whereas the values for pre-deformed and non-deformed LA are not significantly different (**Table 1 and Fig. S3**), suggesting little to no propensity to work hardening of these crystals.

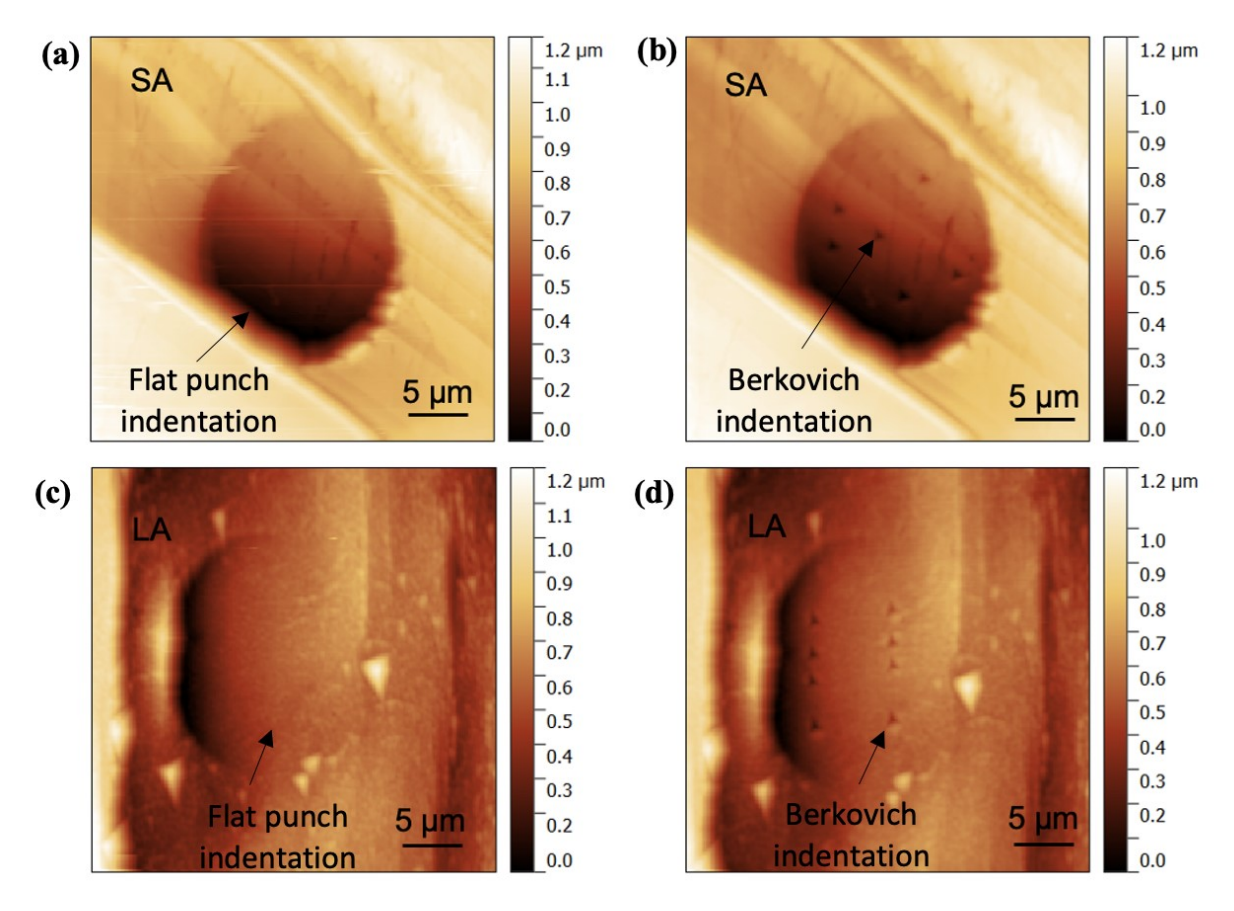


Fig. 6. Surface topography by SPM (a) Deformed area in SA (b) Berkovich indentation on the predeformed area in SA (c) Deformed zone in LA (d) Berkovich indentation on the pre-deformed area in LA.

3.4 Molecular structure analysis and prediction of slip plane

To interpret the differences in mechanical properties, molecular packing of the crystals was analyzed using VESTA. The molecules in SA are arranged in layers when viewed along c-axis (Fig. 7a), from which the slip plane is visually determined to be (020). Within the (020) crystal plane, each SA molecule is bonded to the neighboring molecule by comparatively stronger O-H···O hydrogen bonds (1.72 Å) oriented at an angle with respect to the indentation direction (a-axis) of the SA crystal. On the other hand, weaker C-H···O bonds (2.95 Å) exist between the parallel layers along the b-axis. It is evident that with increasing bond length the bond energies would decrease between the columnar layers and these (020) planes will slide past one another, quite effortlessly, to accommodate the applied load. When indenting on (111) plane in SA, both the O-H···O and C-H···O bonds are now lying perpendicular to the loading direction making the

(111) plane stiffer. Also, the weaker C-H···O bonds are present between the stack of molecular layers oriented at an angle with respect to the indentation axis (**Fig. 7b**).



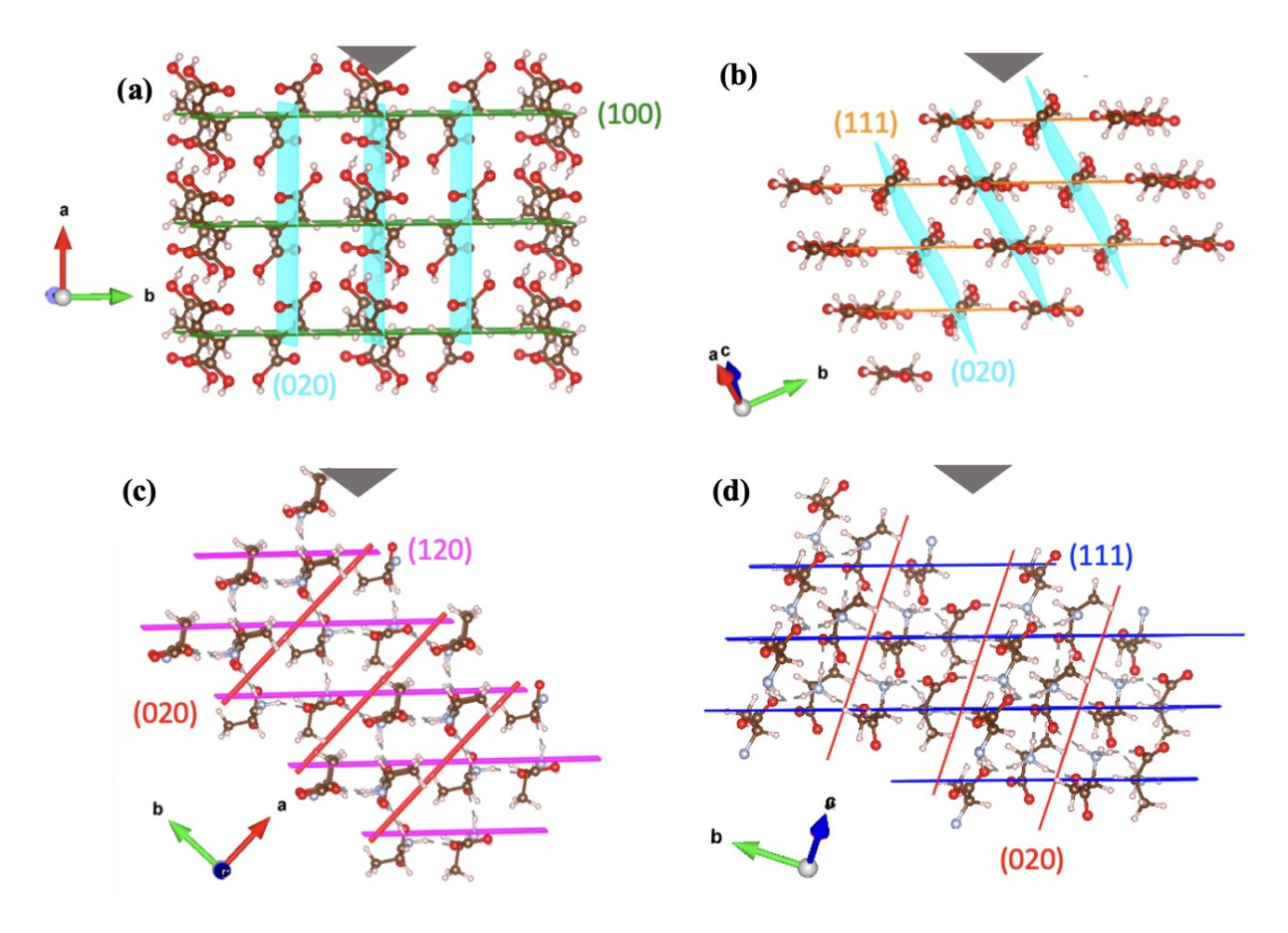


Fig. 7. Molecular packing arrangement in (a) SA along [100], green line shows the trace of (100) plane (b) SA along [111], orange line shows the trace of (111) plane. The slip plane (020) in SA is shown by cyan slabs (c) LA along [120], pink slab shows the trace of (120) plane (d) LA along [111], blue line shows the trace of (111) plane. The slip plane (020) in LA is shown by red lines. The triangle at the top indicates indentation direction. The atoms in red, brown, pink and blue represents oxygen, carbon, hydrogen and nitrogen, respectively.

The indentation modulus, which is a measure of resistance to elastic deformation and depends on bonding interaction or stiffness, is thus lower in (100) due to the presence of weaker C-H···O bonds on the surface perpendicular to the indentation axis. In contrast, indentation on (111) plane requires compressing both the O-H···O and C-H···O bonds resulting in higher E (Fig S4). A similar trend has been observed when measuring the hardness in (100) and (111) planes in SA. Hardness is a measure of resistance to plastic deformation and depends on the shear strength of

the planes, which in turn is a function of bond direction and length. Plastic deformation is known to be favored under applied shear stresses as opposed to normal stresses, so the 3-dimensional stress state under an indenter will provide shear components to induce plastic slip. When indenting the (100) face, the slip plane (020) lies parallel to the indentation axis and is connected by weaker and longer H-bonds. Upon reaching the critical load for initiating plastic deformation, the H-bonds break and the (020) planes undergo facile slip to accommodate the shape of the indenter probe. For the (111) face, the stronger O-H···O bonds now lie perpendicular to the indentation direction along with the C-H···O bonds (**Fig. 7b**) and the orientation of the compact direction is not as favorable as that in (100). This is why (111) exhibits slightly higher *H* than that of (100) in SA. Therefore, the key factor resulting in anisotropy in the structure of SA is the arrangement of the stronger directional H-bonds relative to the loading direction.

LA is an amino acid possessing several strong N-H···O and weak C-H···O hydrogen bonds between the molecules. This results in a three-dimensional network of H-bonds in the LA crystal structure. From visual inspection, both (120) and (020) appear to be the slip plane in LA (Fig. 7c) as gliding along these planes appears feasible due to the lower density of molecular layers. Presence of H-bonds can be observed along all the three axes giving it a relatively isotropic structure. While indenting on the plane (120), the three-dimensional bonding structure and presence of stronger N-H···O bonds strongly resist the elastic and plastic deformation, resulting in comparatively much higher E and H than SA. Similar molecular packing and bonding are present when indenting on (111) plane (Fig. 7d). In both cases, the slip plane (020) lies oblique to the indentation axis. The differences in the E and H values across the two faces of LA is due to the fact that the stronger N- H···O bonds lie both parallel and perpendicular to the load (Fig. 7c), while indenting on (120) making it harder to compress and deform plastically. The orientation of the bonds become angular while indenting on (111) plane (Fig. 7d). Hence, the resolved shear stress on these bonds is higher causing them to break apart at a comparatively lower load resulting in lower E and H than (120). So far in this study, the mechanical responses obtained in different crystal faces have been successfully tied to their underlying crystal structures.

Prediction of slip plane by visualization method may not be always reliable (Wang and Sun, 2018). Thus, slip plane prediction by other methods, such as attachment energy (E_{att}) calculation, has been

investigated (Roberts et al., 1994, Bandyopadhyay and Grant, 2002). Attachment energy is defined as the energy released per mole when a new layer of molecule attaches on the existing growing crystal face. The plane with the lowest absolute value of the attachment energy is the weakest plane and act as the primary slip plane (Wang and Sun, 2018). It was shown that, among the various force fields in Materials Studio, the Dreiding force field works best for molecular crystals in predicting slip planes (Wang et al., 2017, Sun and Kiang, 2008). Here, the attachment energy calculation showed that the (020) plane possesses the lowest E_{att} in both SA and LA (**Table S1 and S2**), affirming the predictions of slip plane by visualization method.

Furthermore, slip planes can be influenced by the surface roughness which can impede the slip of planes relative to one another. The CSD Python API tool in Mercury software offers calculation of surface roughness in terms of rugosity, which is defined as the ratio of the surface area to the projected area and is a descriptor of the physical roughness of the surface. Lower value of rugosity, close to 1, indicates smoother surface and easier slip (Moldovan and Maloney, 2024). Calculation of rugosity of SA (020) yields a value of 1.129 and that of LA (020) is 1.233, (**Fig. S5**), which corresponds to slightly higher layer roughness and hindrance to slip plane movement in LA and support the observance of higher *E* and *H*.

3.5 Intermolecular interaction energy analysis by energy framework model

Crystal structures and the slip planes can also be interpreted in terms of 'energy framework', where interaction energies are graphically and quantitively represented by cylinders that connect the centers of two adjacent molecules (Turner et al., 2015, Mackenzie et al., 2017). This method provides a more reliable way of calculating energies than that of force fields used for calculating E_{att} . Here, the slip planes are identified by calculating the interlayer and intralayer energies. The plane with the highest intralayer and the lowest interlayer interaction energies are depicted as the slip plane (Wang and Sun, 2018). The model calculates the interaction energies between a pair of molecules but the summation of interlayer or intralayer energies between a given molecule and its neighboring molecules are manually calculated to interpret the overall interaction behavior in the crystal structure.

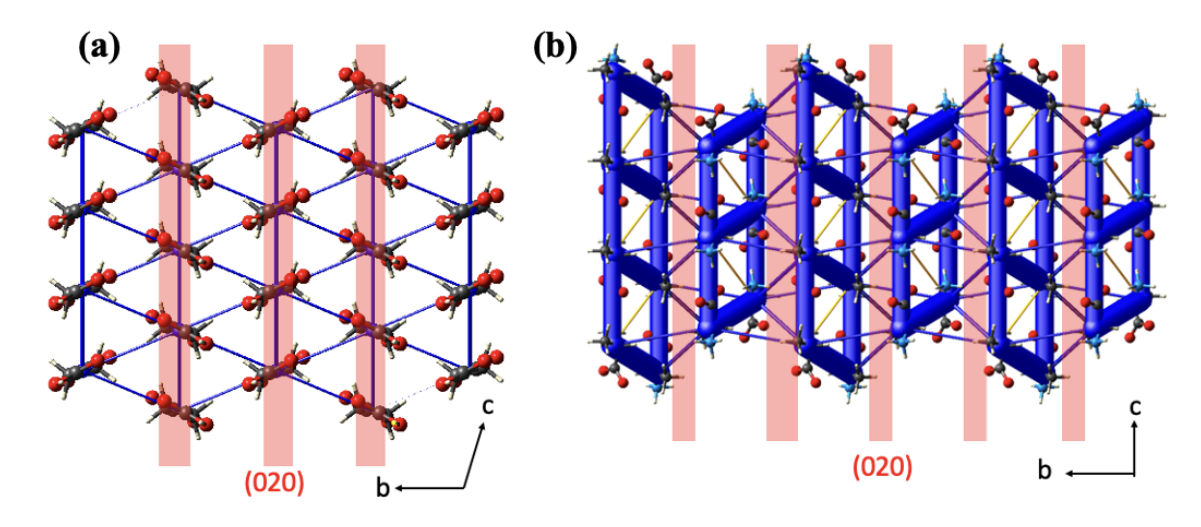


Fig. 8. Energy framework of (a) SA and (b) LA showing likely slip planes shaded in red and strength of intermolecular interactions with the blue cylindrical bars. The energy threshold for the energy framework is set at 0 kJ/mol.

The energy frameworks of SA and LA are significantly different as can be seen from **Fig. 8**. Previously, from the visualization method, we have stated that the adjacent layers of (020) planes are weakly held by C-H···O bonds. From the energy framework model, we can now quantify the energies to be -11.8, -17.9, -6.6, and -0.5 kJ/mol (**Table S3**), whereas along the (020) planes there exist stronger O-H···O bonds with high interaction energy of -67.1 kJ/mol, making SA anisotropic. Calculation of interlayer interaction energy between (020) planes revealed that it is lower (-98.2 kJ/mol) than that within the plane (-134.2 kJ/mol). Due to these weak interaction energies between the adjacent layers of (020), sliding between the planes become energetically favorable. Thus, the energy framework model also supports the assignment of (020) as the slip plane in SA.

Much higher intermolecular interaction energies (-146.8 kJ/mol), shown by the thicker cylindrical bar, are observed along all the directions of LA in **Fig 8b**. There exist weaker bonding interactions (23.5 kJ/mol) across the (020) layers making it the most probable slip plane in LA. Also, the rough topology of the surface layers, as quantified in the previous section, hinders facile slip and plastic deformation rendering a higher E and H in LA. This kind of relatively isotropic and strong energy framework (**Table S4**) is consistent with the high E ranging from ~19-25 GPa and H from ~1-2 GPa. Thus, the methods of visualization, attachment energy calculation, and energy framework

have collectively established the (020) as the likely slip plane in both SA and LA. The experimentally observed higher plasticity of SA than LA by nanoindentation is corroborated by the analyses of their crystal structures using various well-established methods.

426

427

428

429

430

423

424

425

Overall, the findings of this study will contribute to the real-world pharmaceutical manufacturing processes by enriching the database of structure-property relationship in molecular crystals, which will be eventually used in modeling tableting and compaction behaviors as seen in earlier works (Bandyopadhyay and Grant, 2002, Sun and Grant, 2001).

431

432

433

434

435

436

437

438

439

440

441

442

443

444

445

446

447

448

449

450

451

452

453

4. Conclusion

The mechanical properties (E and H) of two different crystal faces of succinic acid and L-alanine were investigated using nanoindentation. L-alanine is stiffer and harder than succinic acid as given by its higher E and H. These values will serve as a guiding tool when selecting crystals for milling and tableting operations in drug manufacturing. L-alanine is expected to undergo size reduction faster whereas succinic acid is expected to have better tabletability owing to its plastic nature. It has been observed that the (111) plane of SA is stiffer (higher E) than (100) showing anisotropic behavior in SA. On the other hand, LA shows more consistent values of E and H across different crystal planes. Work hardening has also found to be negligible in these molecular crystals. Predeformed samples did not exhibit any notable increase in hardness, which is an important indicator that these crystals will retain the same mechanical properties throughout different processing operations. To delve further into the understanding of the mechanical responses of SA and LA, we studied the crystal packing arrangement and found strong correlation between the structure and their mechanical properties. Presence of strong, directional H-bond along the indentation direction and weak interaction between the slip planes in SA makes plastic deformation convenient, resulting in lower E and H. For LA, strong three-dimensional H-bond network with high intermolecular interaction energy hindered facile plastic deformation, making it stiffer and harder. Notably, such a correlation between crystal structure and mechanical property is promising in understanding how mechanical properties impact millability and tabletability as these processes are heavily dependent on the mechanical properties of the crystals. Apart from nanoindentation, in situ SEM micropillar compression testing can obtain stress-strain relationship and provide information on plastic deformation and yield strength in materials. The knowledge depicted here

will benefit the effort of designing crystals with desired mechanical properties, selecting the appropriate form of crystals for a particular application, and reducing the drug development time.

Acknowledgements

We thank the National Science Foundation for support through the Industry University Collaborative Research Center grant IIP-2137264, Center for Integrated Materials Science and Engineering for Pharmaceutical Products (CIMSEPP). Discussion and interaction with Dr. Chenguang Wang on crystal growth is greatly appreciated. We are also grateful to the Characterization facility of the University of Minnesota, which receives partial support from the NSF through the MRSEC (Award Number DMR-2011401) and the NNCI (Award Number ECCS-2025124) programs, for their characterization support.

References

Bandyopadhyay, R., & Grant, D. J. (2002). Plasticity and slip system of plate-shaped crystals of L-lysine monohydrochloride dihydrate. *Pharmaceutical research*, *19*, 491-496. https://doi.org/10.1023/A:1015151830473

Bhukkal, S., Sinha, N., Yadav, H., Goel, S., Singh, B., Bdikin, I., & Kumar, B. (2018). Glycine glutaric acid cocrystals: Morphological, optical, dielectric and mechanical properties via nanoindentation. *Vacuum*, *154*, 90-100. https://doi.org/10.1016/j.vacuum.2018.04.043

Bolshakov, A. P. G. M., & Pharr, G. M. (1998). Influences of pileup on the measurement of mechanical properties by load and depth sensing indentation techniques. *Journal of materials research*, *13*(4), 1049-1058. https://doi.org/10.1557/JMR.1998.0146

Burch, A. C., Yeager, J. D., & Bahr, D. F. (2017). Nanoindentation of HMX and idoxuridine to determine mechanical similarity. *Crystals*, 7(11), 335. https://doi.org/10.3390/cryst7110335

Burch, A. C., Wilde, Z. R., Bahr, D. F., & Yeager, J. D. (2020). A thermal and nanomechanical study of molecular crystals as versatile mocks for pentaerythritol tetranitrate. *Crystals*, 10(2), 126. https://doi.org/10.3390/cryst10020126

Chattoraj, S., Shi, L., & Sun, C. C. (2010). Understanding the relationship between crystal structure, plasticity and compaction behaviour of theophylline, methyl gallate, and their 1: 1 co-crystal. *CrystEngComm*, *12*(8), 2466-2472. https://doi.org/10.1039/C000614A

Clarebrough, L. M., & Hargreaves, M. E. (1959). Work hardening of metals. *Progress in Metal Physics*, 8, 1-103. https://doi.org/10.1016/0502-8205(59)90013-9

- Dassault Systèmes BIOVIA, Materials Studio, 7.0, 2022
- Datta, S., & Grant, D. J. (2004). Crystal structures of drugs: advances in determination, prediction and engineering. *Nature Reviews Drug Discovery*, *3*(1), 42-57. https://doi.org/10.1038/nrd1280
- Duncan-Hewitt, W. C., & Weatherly, G. C. (1989). Evaluating the hardness, Young's modulus and fracture toughness of some pharmaceutical crystals using microindentation techniques. *Journal of materials science letters*, 8(11), 1350-1352. https://doi.org/10.1007/BF00721518
- Egart, M., Ilić, I., Janković, B., Lah, N., & Srčič, S. (2014). Compaction properties of crystalline pharmaceutical ingredients according to the Walker model and nanomechanical attributes. International Journal of Pharmaceutics, 472(1-2), 347-355. https://doi.org/10.1016/j.ijpharm.2014.06.047
- Fischer-Cripps, A. C., & Nicholson, D. W. (2004). Nanoindentation. Mechanical engineering series. Appl. Mech. Rev., 57(2), B12-B12. https://doi.org/10.1115/1.1704625
- Gale, J. D., & Achuthan, A. (2014). The effect of work-hardening and pile-up on nanoindentation measurements. *Journal of materials science*, *49*, 5066-5075. https://doi.org/10.1007/s10853-014-8213-4
- Gopalan, R. S., Kumaradhas, P., Kulkarni, G. U., & Rao, C. N. R. (2000). An experimental charge density study of aliphatic dicarboxylic acids. *Journal of Molecular Structure*, *521*(1-3), 97-106. https://doi.org/10.1016/S0022-2860(99)00293-8
- Gopalan, R. S., Kumaradhas, P., Kulkarni, G. U., & Rao, C. N. R. (2000). An experimental charge density study of aliphatic dicarboxylic acids. *Journal of Molecular Structure*, *521*(1-3), 97-106. https://doi.org/10.1016/S0022-2860(99)00293-8
- Grennan, H. P., Burch, A. C., Tappan, B. C., Manner, V. W., & Bahr, D. F. (2023). Addressing nanomechanical testing irregularities in molecular organic crystals to determine mechanical properties. *Journal of Materials Research*, 38(19), 4431-4440.
- Groom, C. R., Bruno, I. J., Lightfoot, M. P., & Ward, S. C. (2016). The Cambridge structural database. *Acta Crystallographica Section B: Structural Science, Crystal Engineering and Materials*, 72(2), 171-179. https://doi.org/10.1107/S2052520616003954
- Johnson, K. L. (1982). One hundred years of Hertz contact. Proceedings of the Institution of Mechanical Engineers, 196(1), 363-378. https://doi.org/10.1243/PIME_PROC_1982_196_039_02
- Khan, M., & Picu, C. R. (2021). Strain hardening in molecular crystal cyclotetramethylenetetranitramine (β-HMX): a theoretical evaluation. *Modelling and Simulation in Materials Science and Engineering*, 29(7), 075010. https://doi.org/10.1088/1361-651X/ac22ed

- Kiran, M. S. R. N., Varughese, S., Reddy, C. M., Ramamurty, U., & Desiraju, G. R. (2010). Mechanical anisotropy in crystalline saccharin: nanoindentation studies. Crystal growth & design, 10(10), 4650-4655. https://doi.org/10.1021/cg1009362
- Kumar Bandaru, R., Rout, S. R., Kenguva, G., Gorain, B., Alhakamy, N. A., Kesharwani, P., & Dandela, R. (2021). Recent advances in pharmaceutical cocrystals: From bench to market. *Frontiers in Pharmacology*, *12*, 780582. https://doi.org/10.3389/fphar.2021.780582
- Liao, X., & Wiedmann, T. S. (2005). Measurement of process-dependent material properties of pharmaceutical solids by nanoindentation. *Journal of pharmaceutical sciences*, 94(1), 79-92. https://doi.org/10.1002/jps.20227
- Liu, F., Hooks, D. E., Li, N., Mara, N. A., & Swift, J. A. (2018). Mechanical properties of anhydrous and hydrated uric acid crystals. *Chemistry of Materials*, *30*(11), 3798-3805. https://doi.org/10.1021/acs.chemmater.8b00939
- Lorenz, D., Zeckzer, A., Hilpert, U., Grau, P., Johansen, H., & Leipner, H. S. (2003). Pop-in effect as homogeneous nucleation of dislocations during nanoindentation. *Physical review B*, 67(17), 172101. https://doi.org/10.1103/PhysRevB.67.172101
- Mackenzie, C. F., Spackman, P. R., Jayatilaka, D., & Spackman, M. A. (2017). CrystalExplorer model energies and energy frameworks: extension to metal coordination compounds, organic salts, solvates and open-shell systems. *IUCrJ*, *4*(5), 575-587. https://doi.org/10.1107/S205225251700848X
- Macrae, C. F., Bruno, I. J., Chisholm, J. A., Edgington, P. R., McCabe, P., Pidcock, E., Rodriguez-Monge, L., Taylor, R., Streek, J.V.D. and Wood, P. A. (2008). Mercury CSD 2.0–new features for the visualization and investigation of crystal structures. *Journal of Applied Crystallography*, *41*(2), 466-470. https://doi.org/10.1107/S0021889807067908
- Majumder, S., Sun, C. C., & Mara, N. A. (2022). Nanomechanical testing in drug delivery: Theory, applications, and emerging trends. *Advanced Drug Delivery Reviews*, *183*, 114167. https://doi.org/10.1016/j.addr.2022.114167
- Malaj, L., Censi, R., Gashi, Z., & Di Martino, P. (2010). Compression behaviour of anhydrous and hydrate forms of sodium naproxen. *International journal of pharmaceutics*, 390(2), 142-149. https://doi.org/10.1016/j.ijpharm.2010.01.036
- Maughan, M. R., Carvajal, M. T., & Bahr, D. F. (2015). Nanomechanical testing technique for millimeter-sized and smaller molecular crystals. *International Journal of Pharmaceutics*, 486(1-2), 324-330. https://doi.org/10.1016/j.ijpharm.2015.03.062
- Meier, M., John, E., Wieckhusen, D., Wirth, W., & Peukert, W. (2009). Influence of mechanical properties on impact fracture: Prediction of the milling behaviour of pharmaceutical powders by nanoindentation. *Powder Technology*, *188*(3), 301-313. https://doi.org/10.1016/j.powtec.2008.05.009

- Mishra, M. K., Ramamurty, U., & Desiraju, G. R. (2016). Mechanical property design of molecular solids. *Current Opinion in Solid State and Materials Science*, *20*(6), 361-370. https://doi.org/10.1016/j.cossms.2016.05.011
- Mitchell, T. E., Foxall, R. A., & Hirsch, P. B. (1963). Work-hardening in niobium single crystals. *Philosophical Magazine*, 8(95), 1895-1920. https://doi.org/10.1080/14786436308209081
- Modi, S. R., Dantuluri, A. K., Perumalla, S. R., Sun, C. C., & Bansal, A. K. (2014). Effect of crystal habit on intrinsic dissolution behavior of celecoxib due to differential wettability. *Crystal growth & design*, 14(10), 5283-5292. https://doi.org/10.1021/cg501084a
- Mohamed, R. M., Mishra, M. K., Al-Harbi, L. M., Al-Ghamdi, M. S., & Ramamurty, U. (2015). Anisotropy in the mechanical properties of organic crystals: temperature dependence. *RSC Advances*, 5(79), 64156-64162. https://doi.org/10.1039/C5RA11656B
- Moldovan, A. A., & Maloney, A. G. (2024). Surface Analysis—From Crystal Structures to Particle Properties. *Crystal Growth & Design*, 24, 4160-4169. https://doi.org/10.1021/acs.cgd.4c00259
- Momma, K., & Izumi, F. (2011). VESTA 3 for three-dimensional visualization of crystal, volumetric and morphology data. *Journal of applied crystallography*, 44(6), 1272-1276. https://doi.org/10.1107/S0021889811038970
- Mondal, P. K., Bhandary, S., Javoor, M. G., Cleetus, A., Mangalampalli, S. K., Ramamurty, U., & Chopra, D. (2020). Probing the distinct nanomechanical behaviour of a new co-crystal and a known solvate of 5-fluoroisatin and identification of a new polymorph. *CrystEngComm*, 22(15), 2566-2572. https://doi.org/10.1039/C9CE01659G
- Nabarro, F. R. N. (1989). Work hardening and dynamical recovery of FCC metals in multiple glide. *Acta metallurgica*, 37(6), 1521-1546. https://doi.org/10.1016/0001-6160(89)90122-3
- Necas, D. (2012). Gwyddion: an open-source software for SPM data analysis. *Cent Eur J Phys*, 10, 181.
- Oliver, W. C., & Pharr, G. M. (1992). An improved technique for determining hardness and elastic modulus using load and displacement sensing indentation experiments. *Journal of materials research*, 7(6), 1564-1583. https://doi.org/10.1557/JMR.1992.1564
- Rajkumar, A. D., Reynolds, G. K., Wilson, D., Wren, S. A., & Salman, A. D. (2019). The effect of roller compaction and tableting stresses on pharmaceutical tablet performance. *Powder technology*, *341*, 23-37. https://doi.org/10.1016/j.powtec.2018.08.065

- Ramos, K. J., & Bahr, D. F. (2007). Mechanical behavior assessment of sucrose using nanoindentation. *Journal of materials research*, 22(7), 2037-2045. https://doi.org/10.1557/jmr.2007.0249
- Ramos, K. J., Hooks, D. E., & Bahr, D. F. (2009). Direct observation of plasticity and quantitative hardness measurements in single crystal cyclotrimethylene trinitramine by nanoindentation. *Philosophical Magazine*, 89(27), 2381-2402. https://doi.org/10.1080/14786430903120335
- Reddy, C. M., Krishna, G. R., & Ghosh, S. (2010). Mechanical properties of molecular crystals—applications to crystal engineering. *CrystEngComm*, *12*(8), 2296-2314. https://doi.org/10.1039/C003466E
- Roberts, R. J., Rowe, R. C., & York, P. (1994). The relationship between indentation hardness of organic solids and their molecular structure. *Journal of materials science*, *29*, 2289-2296. https://doi.org/10.1007/BF00363416
- Sanphui, P., Mishra, M. K., Ramamurty, U., & Desiraju, G. R. (2015). Tuning mechanical properties of pharmaceutical crystals with multicomponent crystals: voriconazole as a case study. *Molecular Pharmaceutics*, *12*(3), 889-897. https://doi.org/10.1021/mp500719t
- Schuh, C. A. (2006). Nanoindentation studies of materials. *Materials today*, *9*(5), 32-40. https://doi.org/10.1016/S1369-7021(06)71495-X
- Spackman, P. R., Turner, M. J., McKinnon, J. J., Wolff, S. K., Grimwood, D. J., Jayatilaka, D., & Spackman, M. A. (2021). CrystalExplorer: A program for Hirshfeld surface analysis, visualization and quantitative analysis of molecular crystals. *Journal of Applied Crystallography*, *54*(3), 1006-1011. https://doi.org/10.1107/S1600576721002910
- Storey, R. A., & Ymén, I. (Eds.). (2011). *Solid state characterization of pharmaceuticals*. John Wiley & Sons.
- Sun, C. C., & Kiang, Y. H. (2008). On the identification of slip planes in organic crystals based on attachment energy calculation. *Journal of pharmaceutical sciences*, 97(8), 3456-3461. https://doi.org/10.1002/jps.21234
- Sun, C. C., & Kleinebudde, P. (2016). Mini review: Mechanisms to the loss of tabletability by dry granulation. *European Journal of Pharmaceutics and Biopharmaceutics*, 106, 9-14. https://doi.org/10.1016/j.ejpb.2016.04.003
- Sun, C., & Grant, D. J. (2001). Influence of crystal shape on the tableting performance of L-lysine monohydrochloride dihydrate. *Journal of pharmaceutical sciences*, *90*(5), 569-579. https://doi.org/10.1002/1520-6017(200105)90:5%3C569::AID-JPS1013%3E3.0.CO;2-4

- Sun, C., & Grant, D. J. (2004). Improved tableting properties of p-hydroxybenzoic acid by water of crystallization: a molecular insight. *Pharmaceutical research*, *21*, 382-386. https://doi.org/10.1023/B:PHAM.0000016272.81390.b4
- Taw, M. R., Yeager, J. D., Hooks, D. E., Carvajal, T. M., & Bahr, D. F. (2017). The mechanical properties of as-grown noncubic organic molecular crystals assessed by nanoindentation. *Journal of Materials Research*, 32(14), 2728-2737. https://doi.org/10.1557/jmr.2017.219
- Taylor, L. J., Papadopoulos, D. G., Dunn, P. J., Bentham, A. C., Dawson, N. J., Mitchell, J. C., & Snowden, M. J. (2004). Predictive milling of pharmaceutical materials using nanoindentation of single crystals. *Organic process research & development*, 8(4), 674-679. https://doi.org/10.1021/op0300241
- Turner, M. J., Thomas, S. P., Shi, M. W., Jayatilaka, D., & Spackman, M. A. (2015). Energy frameworks: insights into interaction anisotropy and the mechanical properties of molecular crystals. *Chemical Communications*, *51*(18), 3735-3738. https://doi.org/10.1039/C4CC09074H
- Varughese, S., Kiran, M. S. R. N., Ramamurty, U., & Desiraju, G. R. (2013). Nanoindentation in crystal engineering: quantifying mechanical properties of molecular crystals. *Angewandte Chemie International Edition*, 52(10), 2701-2712. https://doi.org/10.1002/anie.201205002
- Wang, C., & Sun, C. C. (2018). Identifying slip planes in organic polymorphs by combined energy framework calculations and topology analysis. *Crystal Growth & Design*, 18(3), 1909-1916. https://doi.org/10.1021/acs.cgd.8b00202
- Wang, C., Paul, S., Wang, K., Hu, S., & Sun, C. C. (2017). Relationships among crystal structures, mechanical properties, and tableting performance probed using four salts of diphenhydramine. *Crystal Growth & Design*, *17*(11), 6030-6040. https://doi.org/10.1021/acs.cgd.7b01153
- Wilson, C. C., Myles, D., Ghosh, M., Johnson, L. N., & Wang, W. (2005). Neutron diffraction investigations of L-and D-alanine at different temperatures: the search for structural evidence for parity violation. *New Journal of Chemistry*, *29*(10), 1318-1322. https://doi.org/10.1039/B419295H
- Wilson, C. C., Myles, D., Ghosh, M., Johnson, L. N., & Wang, W. (2005). Neutron diffraction investigations of L-and D-alanine at different temperatures: the search for structural evidence for parity violation. *New Journal of Chemistry*, *29*(10), 1318-1322. https://doi.org/10.1039/B419295H
- Zepeda-Ruiz, L. A., Stukowski, A., Oppelstrup, T., Bertin, N., Barton, N. R., Freitas, R., & Bulatov, V. V. (2021). Atomistic insights into metal hardening. *Nature materials*, 20(3), 315-320. https://doi.org/10.1038/s41563-020-00815-1